Numerical Study of the Shock Wave Propagation in a Micron-Scale Contracting Channel

G.V. Shoev[a], Ye.A. Bondar[a], D.V. Khotyanovsky[a], A.N. Kudryavtsev[a], G. Mirshekari[b], M. Brouillette[b] and M.S. Ivanov[a]

[a]*Khristianovich Institute of Theoretical and Applied Mechanics, Institutskaya 4/1, Novosibirsk, Russia, 630090*

[b]*Department of Mechanical Engineering, Université de Sherbrooke, Sherbrooke, Canada J1K 2R1*

Abstract. Entry of a shock wave into a microchannel and its propagation in the channel are studied numerically by the continuum and kinetic approaches. It is shown that the shock wave is amplified immediately after it enters the microchannel. After that, the shock wave in an inviscid computation propagates over the microchannel with a constant velocity. In a viscous computation, the shock wave velocity decreases and the wave attenuates. Qualitative agreement between experimental data and viscous computations is demonstrated.

Keywords: Shock wave propagation on microscales, viscosity effects.
PACS: 47.45.Gx, 47.40.Ki

INTRODUCTION

The interest in the microscale flow behavior has increased during the last two decades owing to rapid progress in micromachining techniques. The effects of viscosity and heat conduction, heat losses due to the wall heat transfer, as well as nonequilibrium phenomena can play an important role in microflows. Recent numerical investigations of shock wave propagation in a microchannel with allowance for viscosity and rarefaction effects [1] revealed significant differences from the inviscid theory, which ensures a correct description of the majority of specific features of macroflows. In that work, the shock wave was generated by breakdown of a membrane separating high-pressure and low-pressure domains. At the moment, however, such an experiment is not feasible, as was noted in [2]. Nevertheless, an alternative variant of shock wave generation in a microchannel was proposed in [3]. The idea was to generate the shock wave in a conventional shock tube and then make it move from the low-pressure chamber to the microchannel. The numerical studies [3] based on Navier-Stokes computations demonstrated the attenuation of the shock wave in the microchannel. The necessity of further research with due allowance for rarefaction effects was noted in that paper.

A recent experimental study of the shock wave entry and propagation in a contracting channel [4] showed attenuation of the shock inside the microchannel. As was noted in that paper, one possible theoretical explanation of this result can be found in terms of transport losses at the channel entrance and inside it. Nevertheless, full understanding of this process is still unavailable. There may be several reasons responsible for the shock wave attenuation in the microchannel: roughness of the walls, effects of viscosity and heat exchange with the walls, etc.

The basic goal of our research is numerical simulations of the shock wave entry and propagation in a microchannel with due allowance for viscosity and rarefaction effects. In this paper, we use two different simulation approaches: the kinetic approach based on the Boltzmann equation and the continuum approach based on Euler and Navier–Stokes (NS) equations. Euler computations are also necessary for comparisons with viscous simulations to reveal effects of viscosity. In NS computations, the rarefaction effects are taken into account by imposing the velocity slip and temperature jump boundary conditions on solid walls. As the Knudsen number in this research is approximately 8.2×10^{-3} and also due to gas nonequilibrium inside the shock waves, the applicability of NS equations cannot be taken for granted; therefore, Direct Simulation Monte Carlo (DSMC) [5] computations are additionally

performed for verification of numerical data. The DSMC method can be considered as a numerical tool for solving the kinetic Boltzmann equation, which offers an exact description of the internal structure of the shock waves.

NUMERICAL TECHNIQUES AND BOUNDARY CONDITIONS

The computations are conducted with the full two-dimensional Euler, Navier–Stokes (NS) equations and the Direct Simulation Monte Carlo (DSMC) method [5]. The Navier–Stokes code [6] is a time-explicit shock-capturing code based on 5th order WENO reconstruction [7] of convective fluxes and central 4th order approximation of dissipation terms. A structured rectangular grid with refinement in Y-direction inside microchannel and uniform grid in X-direction is used. To model shock wave propagation in Euler and NS computations, conditions corresponding to the Rankine-Hugoniot conditions behind the normal shock wave with the corresponding shock wave Mach number M_{is} are imposed on the left boundary of the computational domain. As the main task of the present work was modeling the shock wave entry and propagation in a microchannel, the inviscid wall conditions (denoted by E in fig. 1) are imposed on the upper boundary of the ordinary channel and on the right boundary of the microchannel.

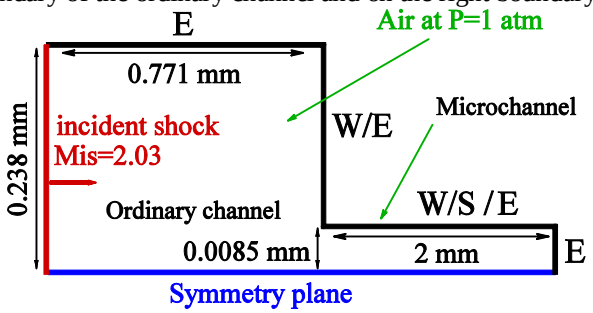

FIGURE 1. Boundary conditions. E - inviscid wall in Euler and NS computations (specular reflection in DSMC computation), W – isothermal wall with no-slip in NS computation (diffuse reflection in DSMC computation), S – isothermal wall with slip in NS computation.

Specific features associated with the boundary layer on the upper wall of the ordinary channel and reflection of the shock wave that entered the microchannel from the right wall are not considered in this study. As shock wave propagation is considered in the present work at small times (~ 3 μs), the isothermal wall conditions are set on the right boundary of the ordinary channel and on the upper boundary of the microchannel. The right boundary of the ordinary channel is subjected to the isothermal no-slip boundary condition (denoted by w in fig. 1). The present study includes two series of computations with different boundary conditions on the upper wall of the microchannel: isothermal no-slip and isothermal slip boundary conditions (denoted by w/s in fig. 1). In Euler computations inviscid walls were used for all boundaries of channels. The computations are started with a uniform flow field corresponding to quiescent gas. The numerical solution is then advanced in time with the third-order Runge–Kutta scheme until the shock wave that entered the microchannel reaches the right wall and reflects from it.

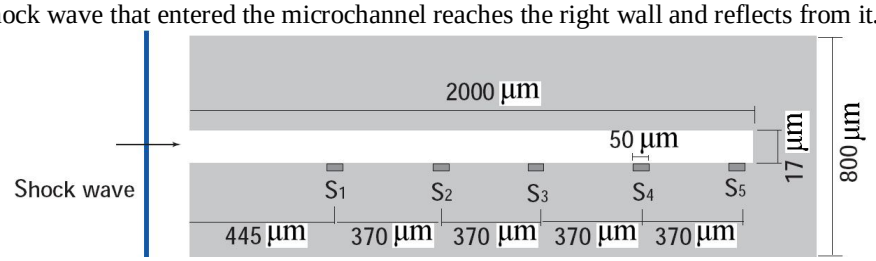

FIGURE 2. Microchannel geometry. The 5 microchannel pressure transducers are denoted as S_1 to S_5.

The DSMC computations are performed by the statistical modeling in low-density environment (SMILE) software system [8] which uses the majorant frequency method for computing collision integrals. The computational domain is similar to the domain used in the NS computations (see fig. 1). The specular reflection conditions (denoted by E in fig. 1) are imposed on the upper boundary of the ordinary channel and on the right boundary of the microchannel. The diffuse reflection model with complete accommodation is applied on the upper wall of the microchannel. Conditions corresponding to the Rankine-Hugoniot conditions behind the normal shock wave with the corresponding shock wave Mach number are imposed on the left boundary of the computational domain. At the initial moment, the domain is populated by the model particles according to the Maxwell distribution function corresponding to the quiescent gas parameters. A uniform rectangular grid is used for modeling molecular collisions and sampling the gas dynamic parameters. Note that a typical computation takes more than 24 hours of computer time with 100 processors.

The power-law dependence of the dynamic viscosity coefficient μ on the temperature T with the exponent ω=0.74 is used in the NS computations. The variable hard-sphere model [5] (VHS) is used in the DSMC computations with the VHS parameter chosen to provide the same dependence of viscosity on temperature. In the DSMC computations flow of the diatomic gas (N_2) with a ratio of specific heats γ=1.4 was used.

The initial data were chosen to be the initial parameters corresponding to the case considered in [4]: M_{is}=2.03, γ=1.4, P_0=1 atm, T_0=293° K, L=8.5 μm, w_c=2 mm, where M_{is} is the Mach number of the incident shock wave (hereinafter, the incident shock wave is understood as the shock wave propagating in the ordinary channel), γ is the ratio of specific heats, P_0 and T_0 are the pressure and temperature of the quiescent gas at the initial time, L is the microchannel half-height, and w_c is the microchannel length. An experiment with the above-mentioned parameters was performed in [4] and provided pressure histories from transducers mounted on the microchannel wall (see fig. 2). In this study the results of Euler and NS computations are compared with the measurements: the pressure values on the wall at points corresponding to each transducer location were calculated at different times.

RESULTS AND DISCUSSION

Figure 3 shows the Mach number fields at different times. The incident shock wave propagating over the ordinary channel ahead of the microchannel entrance is shown in fig. 3a. After the incident wave enters the microchannel, an expansion fan is formed on the microchannel corner (see fig. 3b), in which the gas velocity increases and the flow becomes supersonic.

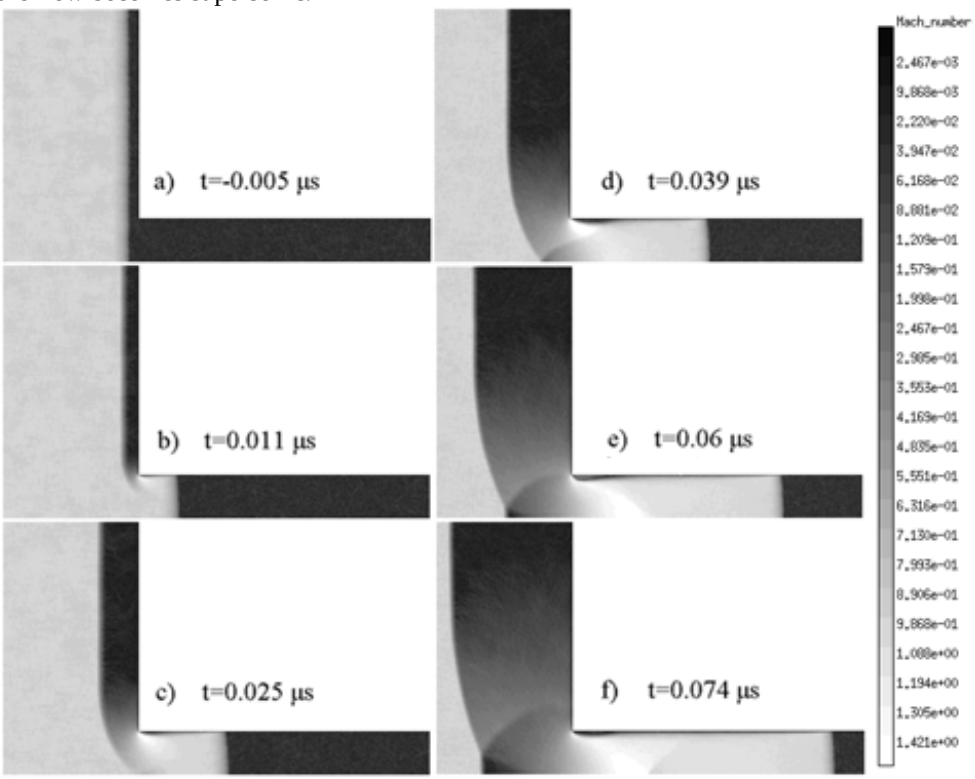

FIGURE 3. Mach number at different time instants. M_{is}=2.03, γ=1.4, P_0=1 atm, T_0=293° K, L=8.5 μm, w_c=2 mm. t=0 corresponds to the instant when the incident shock wave enters the microchannel.

After that (see fig. 3b, 3c), the wave reflected from the corner of the microchannel propagates toward the plane of symmetry. The boundary layer formed on the upper wall of the microchannel is clearly visible beginning from fig. 3c. At the next instant (see fig. 3d), wave reflection occurs on the plane of symmetry, and a configuration similar to a regular configuration of shock waves is formed. It is also well seen in fig. 3d that the shock wave that passed inside the microchannel starts to curve because of its interaction with the upper wall of the microchannel. At the next time instant, the Mach reflection of shock waves is formed in the ordinary channel (fig. 3e), whereas one more wave reflected from the upper wall is seen in the microchannel. In what follows (fig. 3f), the Mach configuration of shock waves persists in the ordinary channel, and the wave reflected at the previous time instant from the upper wall of the

microchannel is now reflected from the axis of symmetry. Thus, the flow behind the shock wave that entered the microchannel is far from being uniform, which may lead to shock wave amplification.

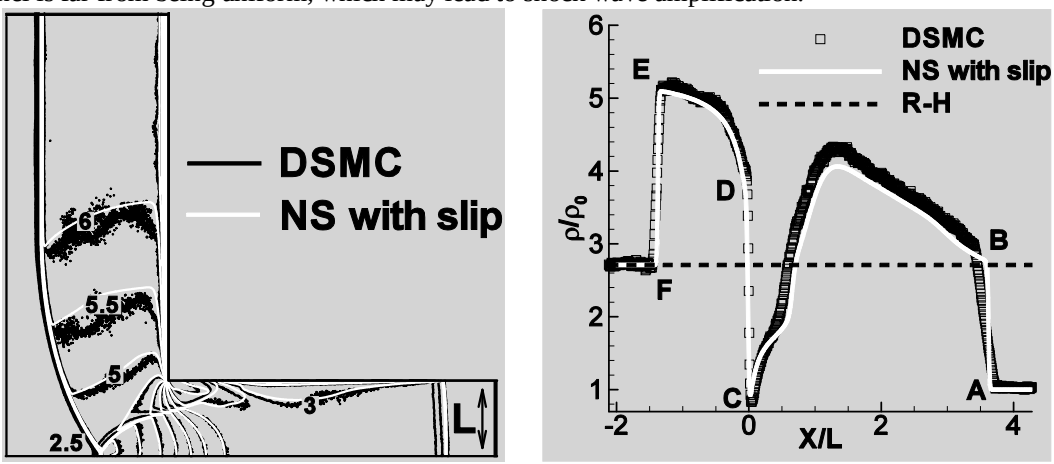

a) Density contours b) Density profiles near the top wall of the microchannel

FIGURE 4. Comparison of DSMC and NS with slip computations. M_{is}=2.03, γ=1.4, P_0=1 atm, T_0=293° K, L=8.5 μm, w_c=2 mm. t=0 corresponds to the instant when the incident shock wave enters the microchannel.

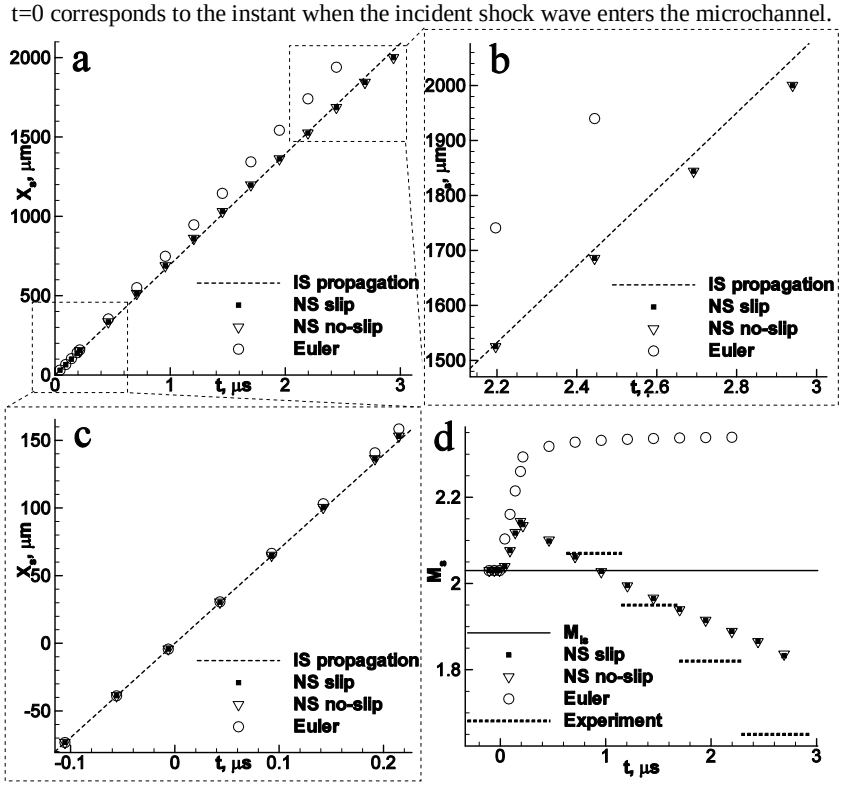

FIGURE 5. Shock wave propagation diagram inside the microchannel. a) (x_s,t) diagram b) zoom for (x_s,t) diagram c) zoom for (x_s,t) diagram d) (M_s,t) diagram

The NS computation with the slip condition and the DSMC computation are compared in fig. 4. Figure 4a shows the density fields, which are in good agreement. Note that the figure shows isolines corresponding to the values of density normalized to the quiescent gas density. A large difference is observed for the thickness of the shock wave that passed inside the microchannel, but the thicknesses of the other shock waves are commensurable. Figure 4b shows the density profiles at constant values of the Y coordinate (Y=L, where L is the microchannel half-height and Y=0 corresponds to the plane of symmetry). The value corresponding to the density behind the incident shock wave is shown by the dotted curve. The segment AB in fig. 4b corresponds to the shock wave that passed inside the microchannel; the segment CD is the expansion fan formed on the corner. The segment FE refers to the shock wave reflected from the right wall of the ordinary channel. It is seen that the density in the microchannel differs substantially from the values corresponding to the Rankine-Hugoniot conditions.

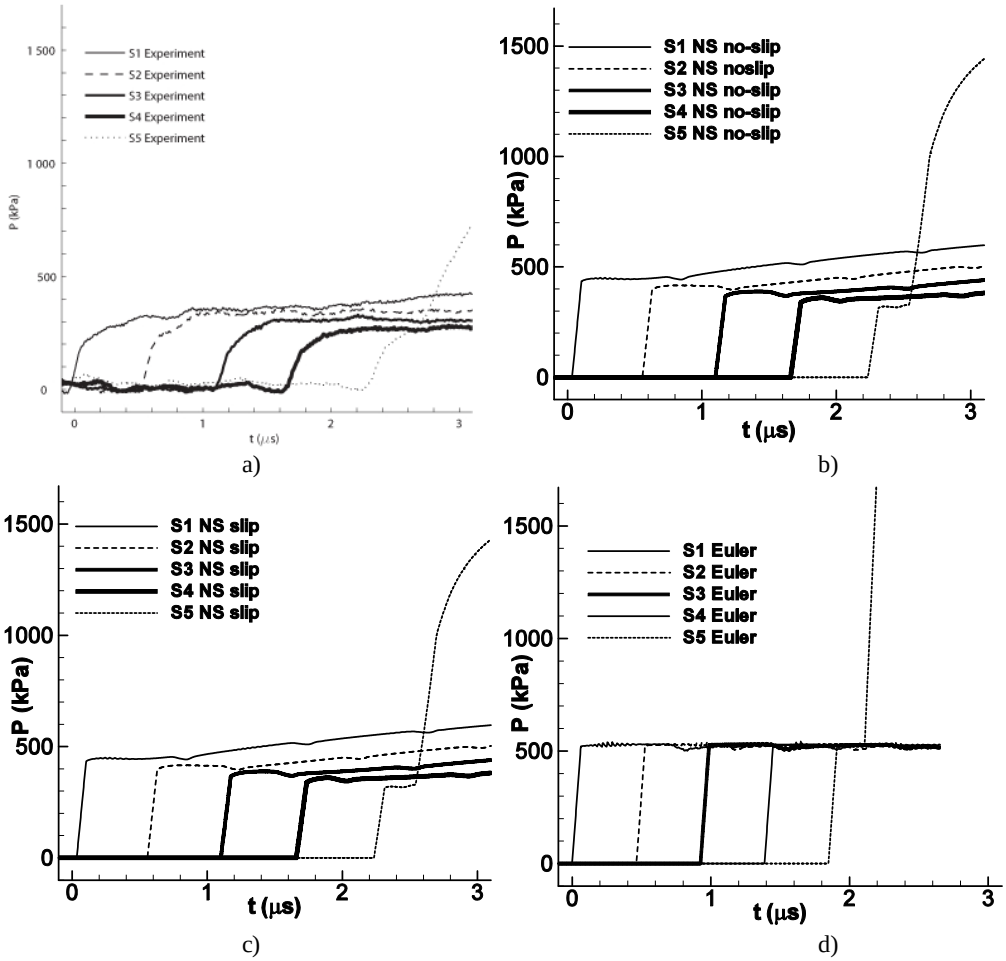

FIGURE 6. Pressure histories in the microchannel. a) Experiment, b) NS computations with no-slip boundary conditions, c) NS computations with slip boundary conditions, d) Euler computation.

The results (see fig. 5) of numerical simulations of shock wave propagation in the microchannel are presented in the form (M_s,t) and (x_s,t), where M_s and x_s are the Mach number and the coordinate of the shock wave propagating in the microchannel, and t is the time. The coordinate system is chosen so that the point (0,0) in the plane (x_s,t) corresponds to the time instant when the incident shock wave reaches the microchannel. It is seen from fig. 5d that the shock wave Mach number increases after the wave enters the microchannel and reaches a maximum value at the point t~0.2 μs. After that, the shock wave starts to attenuate in the viscous computation owing to its interaction with the wall of the microchannel, whereas the shock wave in the inviscid case propagates with a constant velocity. As is seen from the figures, the numerical solutions of the Navier-Stokes equations with different boundary conditions (isothermal no-slip and isothermal slip boundary condition) on the upper wall of the microchannel are practically indistinguishable. The numerical results of the viscous computation on the (x_s,t) diagram practically do not differ from a straight line (dotted curve in fig. 5a, 5b, 5c) corresponding to shock wave propagation with a constant velocity equal to the incident wave velocity. It is worth to note that in viscous case it looks like the effects of viscosity and heat conduction compensate shock wave amplification after entry inside a microchannel and average shock velocity is close to velocity of incident shock. Figure 5d also shows the experimental data [4] for the mean velocity of the shock wave in the microchannel between the pressure transducers. These results allow us to conclude that numerical simulations with allowance for viscosity effects qualitatively agree with the experimental data: the shock wave is amplified immediately behind the microchannel entrance and then decays. It is clearly seen that the experimental data coincide with the viscous computation on the segment t=0.63-1.7 μs. On the segment t=1.7-2.94 μs, however, the experimental data display more intense attenuation of the transmitted shock wave. A possible reason for this discrepancy is three-dimensional effects, which were ignored in numerical simulations.

The pressure histories obtained in numerical simulations and experiments [4] are compared in fig. 6. The zero point on the time axis in these graphs is the time when the shock wave entering the microchannel reaches the left boundary of the first (S1) transducer (see fig. 2). The zero value on the pressure axis corresponds to the quiescent

gas pressure. Figures 6b and 6c show the pressure histories obtained by the numerical solution of Euler and NS equations with no-slip and slip boundary conditions on the top wall of the microchannel. It is seen that there is practically no difference between results of NS computations. The difference (~60 kPa) between the experimental and numerical data in those areas where the shock wave has already passed over the pressure transducers is clearly visible. A possible reason for this difference is three-dimensional effects, which were mentioned above. For the pressure transducer S1, the difference is both qualitative and quantitative. The pressure on the transducer surface permanently increases in the experiment, while numerical simulations predict a small segment (~0.5 μs) with an almost constant pressure. There are also significant differences for the pressure transducer S5: before the shock wave reflection from the right wall of the microchannel, computations give a small segment (~0.1 μs) with an almost constant pressure, whereas the experimental curve has practically no such a segment. It is also clearly seen that inviscid numerical simulation differs substantially from the viscous simulations and experiment – pressure on each transducer is constant and greater than in NS computations and experiment. The shock wave is reflected from the right wall of the microchannel at the point t~2.3 μs. The jump in pressure at this point on the pressure transducer S5 corresponds to the increase in pressure behind the reflected shock wave. The subsequent behavior of the flow in the microchannel was not modeled, because the main goal of this study was to simulate the shock wave entry and its propagation in the microchannel. As a whole, we can state that reasonable agreement for a first simulation was obtained, considering that the actual geometry is more complicated that what is simulated. The microchannel is within a chip that is about 1 mm thick, so there is a flow around the chip and not a reflected shock like at the right boundary of the ordinary channel. At the moment, however, we cannot definitely say whether the flow around the microchannel exerts a strong effect on the flow inside the microchannel and whether this factor leads to a decrease in pressure.

CONCLUSION

The shock wave entry into a microchannel and its propagation in the microchannel at M_{is}=2.03 is studied numerically with the use of the continuum and kinetic approaches. A significant difference between the inviscid and viscous numerical computations is demonstrated. The numerical data obtained show that the shock wave is substantially amplified after it enters the microchannel. After that, the inviscid computation predicts shock wave propagation with a constant velocity, whereas the shock wave in the viscous case starts to attenuate. The results of viscous computations are in qualitative agreement with the experimental data [4], which show shock amplification after it enters the microchannel and its further attenuation.

ACKNOWLEDGMENTS

The research performed at ITAM was supported by the IFS Collaborative Research Project “Numerical studies of the reacting rarefied flows in tubes“, Program No. 11 of the RAS Presidium, Lavrentyev Youth Grant "High-altitude aerothermodynamics of advanced spacecraft taking into account non-equilibrium chemical reactions" and the Russian Foundation for Basic Research (Grant no. 06-01-22000). This support is gratefully acknowledged.

REFERENCES

1. D. E. Zeitoun, Y. Burtschell, I. A. Graur, M. S. Ivanov, A. N. Kudryavtsev, Y. A. Bondar, “Numerical simulation of shock wave propagation in microchannels using continuum and kinetic approaches”, *Shock Waves*, **19**, 307–316 (2009).
2. G. Mirshekari, M. Brouillette, “One-dimensional model for microscale shock tube flow”, *Shock Waves*, **19**, 25-38 (2009).
3. J. D. Parisse, J. Giordano, P. Perrier, Y. Burtschell, I. A. Graur, “Numerical investigation of micro shock waves generation”, *Microfluid Nanofluid*, **6**, 699-709 (2008).
4. G. Mirshekari, M. Brouillette, “Experimental study of the shock propagation in a micron-scale channel”, Proceedings of the 27th ISSW, p. 260, 2009.
5. G. Bird. “Molecular gas dynamics and the direct simulation of gas flows”. Oxford Press, 1994.
6. A. Kudryavtsev, D. Khotyanovsky, “Numerical investigation of high speed free shear flow instability and mach wave radiation”, Int. J. Aeroacoust, **4**, 325–344 (2005).
7. G. Jiang, C Shu, “Efficient Implementation of Weighted ENO Schemes”, J Comput. Phys., **126**, 202–228 (1996).
8. M. Ivanov, G. Markelov, S. Gimelshein, “Statistical simulation of reactive rarefied flows: numerical approach and applications”, AIAA Paper, 98-2669 (1998).